Comparative study of surface-lattice-site resolved neutralization of slow multicharged ions during large-angle quasi-binary collisions with Au(110): Simulation and Experiment

F. W. Meyer and V. A. Morozov

Physics Division, Oak Ridge National Laboratory, Oak Ridge, Tennessee 37831-6372 USA

Abstract

In this article we extend our earlier studies of the azimuthal dependences of low energy projectiles scattered in large angle quasi-binary collisions from Au(110). Measurements are presented for 20 keV Ar^{9+} at normal incidence, which are compared with our earlier measurements for this ion at 5 keV and 10^0 incidence angle. A deconvolution procedure based on MARLOWE simulation results carried out at both energies provides information about the energy dependence of projectile neutralization during interactions just with the atoms along the top ridge of the reconstructed Au(110) surface corrugation, in comparison to, e.g., interactions with atoms lying on the sidewalls. To test the sensitivity of the agreement between the MARLOWE results and the experimental measurements, we show simulation results obtained for a non-reconstructed Au(110) surface with 20 keV Ar projectiles, and for different scattering potentials that are intended to simulate the effects on scattering trajectory of a projectile inner shell vacancy surviving the binary collision. In addition, simulation results are shown for a number of different total scattering angles, to illustrate their utility in finding optimum values for this parameter prior to the actual measurements.

PACS numbers: 79.20.Rf, 79.20.Ap, 34.50 Dy, 61.18.Bn

---

*Corresponding author: FAX: +1-1-865-574-1118
E-mail address: meyerfw@ornl.gov

Introduction

The large angle scattering technique has been used in a number of recent studies [1-5] of multicharged projectile neutralization during interactions with metal and insulator surfaces. By the use of energy and charge analysis of the backscattered projectiles, this method provides, e.g., insights into energy loss mechanisms accompanying projectile neutralization [2], and permits, in contrast to studies of grazing deflection events which result by cumulative scattering involving a large number of lattice sites [6], the resolution of interactions occurring with just one or two atoms located on the target surface.

In this article we have extended our previous studies [3,4] on multicharged projectile neutralization during binary and quasi-binary collisions with atoms located on a Au(110) surface. First, we have measured the target azimuth dependence of scattered charge fractions for 20 keV Ar^{9+} ions normally incident on Au(110), for comparison with similar measurements of 5 keV Ar^{9+} projectiles incident on Au(110) at 10^0. In order to make an analysis of the contributions of the various Au(110) surface scattering sites and collision types similar to that already performed at 5 keV, we also carried out MARLOWE [7] trajectory simulations at the higher projectile energy and normal incidence angle. We report as well the results of some auxiliary MARLOWE studies in which we explored the sensitivity of the trajectory simulations to changes in the scattering potential intended to mimic the effects of incomplete neutralization, and to the surface topography itself, by comparing scattering from both reconstructed and unreconstructed Au(110) surfaces.

As has been noted previously, at the few to tens of keV impact energies studied in the present article, contributions to the overall projectile neutralization by "hollow atom" formation at large distances followed by Auger relaxation prior to surface-impact [8] are considered to be

negligible, and multicharged ion (MCI) neutralization proceeds instead by the complex multi-electron processes occurring closer to the surface in the vicinity of the trajectory turning point. The goal of the present contribution is to demonstrate the potential of the large angle backscattering technique for such MCI-surface charge exchange studies at higher energies, and to explore what additional information the measured azimuth dependences might contain, either regarding the neutralization process or the surface topography itself.

Experiment

The measurements were carried out at the ORNL Multicharged Ion Research Facility with an apparatus that implements an ultra-high vacuum (10^{-10} mbar) floating scattering chamber and time-of-flight (TOF) analyzer with floatable drift tube [9,10,11], permitting simultaneous measurements of energy distributions and charge fractions of projectiles scattered from the single crystal target into 120^0. The target was attached to a sample mount with two rotational degrees of freedom and was prepared by cycles of sputter cleaning under grazing incidence with 2 keV Ar+ ions and successive annealing cycles at about 450^0 C. The chopped primary beams of argon MCI were decelerated from (10 x q) keV to their final energy before impinging on the Au(110) surface.

Figure 1 shows a typical scattered projectile TOF spectrum for 20 keV Ar^{9+} ions incident normally on CsI(100). The figure illustrates the degree of charge state separation obtainable at this energy using the maximum drift tube voltage of –4 kV achievable with the present set-up. As can be seen from the figure, the spectrum exhibits rather sharp peaks originating from *elastic* binary collisions between the incident projectile and individual target atoms. The peaks due to non-neutral scattered charge states sit on the falling slope of a broad structure associated with scattered neutrals that have undergone multiple collisions. The non-neutral binary collision (BC)

peaks are stripped from this 'background' continuum by subtraction of an auxiliary spectrum obtained with the flight tube at zero potential, the result of which is the "difference" spectrum also shown in the figure. Both the shape and intensity of the multiple collision background, as well as the intensities of quasi-binary collision peaks, are strong functions of incidence angle and target azimuthal orientation, as has also been found in the case of singly charged incident ions [12]. The multiple collision background, while being a major structure in the scattered neutral spectra, is not a significant feature in the non-neutral scattered charge state spectra, indicating very low survival probabilities of non-neutral scattered projectiles in multiple collisions for the present case. Prior to determination of the absolute scattered charge fractions shown in a later section, the background-subtracted binary-collision-peak areas of the various scattered charge states are corrected for collection and detection efficiency effects as has been previously described [10].

Computer Trajectory Simulations

To understand incidence angle and target azimuthal orientation dependences of the scattered fluxes, projectile trajectory simulations using the MARLOWE (version 14c) code [7] were carried out. MARLOWE treats the interaction between the projectile and the surface in an e*lastic* binary collision approximation (BCA). An exponential-sum screened Coulomb interaction potential was chosen with default parameters from Ref. 13, and a (2x1) reconstruction of the Au(110) surface was assumed [14,15]. The primary beam energy distribution was simulated in a series of MARLOWE tasks with different initial particle kinetic energies. Due to computing time constraints the angular acceptance was increased by a factor of 4 over the experimental acceptance angle of 2^0. Of the 4×10^6 trajectories generated for each target orientation investigated, about (0.03 - 0.08) % were scattered into the detector acceptance cone.

For the latter trajectories, the number of collisions, scattering angles, etc. were saved, permitting their subsequent reconstruction.

The simulations were used as the basis for analyzing the collision events contributing to the "binary collision" ("BC") peaks seen experimentally. They reveal that the "BC" peak is in fact built up from two kinds of events - pure single **SC** and "quasi-binary" double **DC** collisions. By "quasi-binary" is meant that class of double (and triple) collisions, usually a combination of large angle ("hard") and one or more small angle ("soft") scattering events that do not lie in the same plane, resulting in final energies encompassed in the observed main energy loss peak. The quasi-binary **DC** events are particularly prominent for scattering along the [100] target azimuth direction, i.e. *across* the missing rows of the reconstructed Au(110) surface, as is illustrated in Fig. 2. These collisions are to be distinguished from the true double collisions noted by, e.g. Huang et al. [1], which are evident at higher scattered energies (at ~3200 eV for the case of the 5 keV incident projectiles shown in Fig. 2). Higher multiplicity events (i.e. number of collisions >2) do not contribute to the "BC" peak, and form instead the pedestal upon which the peak sits. As can be seen from the figure, for the particular target azimuth shown, triple collisions contribute to the "true" double collision peak at 3200 eV as well. The relative contributions of true binary and quasi-binary double (and at higher energy, triple) collisions to the "BC" peak vary strongly with target azimuth, and underlie the measured azimuth variations of scattered charge fractions that will be shown in a later section.

An analysis of the target layers in which the events making up the "BC" peak occur for our geometry, shows that single collisions in only the top three target layers contribute. They are denoted **SI**, **SII**, and **SIII**, respectively. Target atoms not directly at the surface/vacuum interface have negligible contribution to the "BC" peak, presumably resulting from shadowing effects due

to our near normal incidence conditions. The "hard"-"soft" quasi-binary collisions originate exclusively from the second and third target layers and will be denoted **DII** and **DIII**, the Roman numeral designating the layer in which the "hard" collision occurs . Fig. 3 shows these 5 collision types as well as their individual target azimuth dependences for 5 keV Ar projectiles incident at 10^0, together with a schematic representation of the (2x1) reconstructed Au(110) surface. A striking feature of the simulation results is that each collision type is characterized by a distinct and unique dependence on target azimuth.

Experimental and Simulation Results at 20 keV

Figure 4 shows the target azimuth dependence of the total (i.e. summed over all scattered charge states) scattered flux as well as that of the individual scattered charge states for 20 keV Ar^{9+} normally incident on Au(110). Figures 5 and 6 show MARLOWE simulation results for the same energy and incidence angle conditions. The simulation results are organized into four panels, corresponding to contributions from the first, second, and third target layers, with the fourth panel showing a comparison between the summed contribution from all three layers and the total observed scattered flux. In Figure 5, the default MARLOWE criterion for a "collision" (maximum impact parameter b_{max}<1.6Å) was used, while in Figure 6, the MARLOWE output was sorted using a slightly more restrictive impact parameter criterion, as discussed in the next section.

Discussion of Experimental and Simulation Results

The experimental results shown in Figure 4 are qualitatively very similar to those shown in Refs. 3 and 4. The neutral scattered charge fraction shows the greatest variation with target azimuth orientation, with primary and secondary maxima in the vicinity of the [110] and [100] directions, respectively, and a miniumum in the azimuth range $40^0 - 70^0$, while the higher

scattered charge fractions show significantly smaller modulation as function of target azimuth. As discussed previously [3,4] and below, these modulations result from the azimuthal variation of the contributions of **SC** and quasi-binary multiple collisions to the formation of a particular final scattered charge state. Figure 5 shows the contributions to the total scattered flux from the first three layers (panels 1-3) broken down by the number of collisions in a particular sequence initiated by a "hard" collision in the identified layer, using the MARLOWE default "collision" criterion (maximum impact parameter b_{max}<1.6Å) . As can be seen in the first panel of the figure, in contrast to our results at 5 keV with 10^0 incidence angle, interactions with the top layer are comprised now of both single and double collisions. This arises from the fact that, for normal incidence and scattering along the [110] direction, the receding projectile passes by the next lattice site along the row (in-plane) with an impact parameter of about 1.4 Å, i.e. less than b_{max}. This impact parameter is significantly greater than that expected for the quasi-binary (out-of-plane) DC events included in the 5 keV simulations when scaled to the higher collision energy considered here. More importantly, the azimuthal dependences of the resulting collision types are no longer as unique as was the case at 5 keV (e.g., DI, DII, and DIII events all show pronounced maxima in the [110] direction, while both SI and SII now show azimuthally flat distributions away from the [100] direction), thus resulting in fits which are themselves no longer as unique as the 5 keV fit results. Given the quasi-binary **DC** impact parameters along the [100] direction at 5 keV of 0.133 Å and 1.14 Å, respectively (see Footnote 19 of Ref. 3), and assuming that neutralization distances decrease with increasing projectile energies, we have performed an alternate sorting of the MARLOWE results, in which the in-plane second MARLOWE collision along the [110] direction is considered as contributing to the **SI**, and not the **DI** collision type. This is tantamount to the assumption that the dominant neutralization channel is only open for

impact parameters less than about. 1.2 Å. Using this more restrictive definition of charge exchange collision, Figure 6 is obtained. As can be seen, the azimuth dependence obtained in the 5 keV MARLOWE simulation for the **SC** and **DC** collision types is nearly recovered. The remaining difference that shows up in both Figs. 5 and 6 is the double maximum found in the vicinity of the [100] direction, which is an additional manifestation of the normal vs. 10^0 incidence angles, showing up in both the observed and simulated azimuth dependences. As can be seen from panel 3 of Figure 6, this double maximum arises mainly from quasi-binary double and triple collisions originating in the second and third layers that become possible over a small range of azimuths on either side of the [100] direction. Note that a new **SII** peak appears in the [100] direction as a consequence of the alternate sorting of MARLOWE events with the more restrictive charge-exchange impact-parameter criterion. It results from the passage on the receding trajectory between two top row lattice sites, and would have remained classified as a **DII** collision type had the additional constraint of in-plane vs. out-of-plane scattering been imposed in the resorting. Such a refinement will be considered in future investigations. We note that this detail had only minor effect on the charge fraction fitting results discussed in the next paragraph. Both Figures 5 and 6 show in the 4^{th} panels comparisons with the total observed scattered flux, (i.e. summed over all charge states). An agreement similar in quality to that obtained at 5 keV is evident. The identical agreement evident in both figures reinforces the fact that the difference between the two simulation results is purely a redistribution of collision types, and therefore does not affect the azimuth distribution of the total scattered flux.

Using the excellent agreement of the total observed and simulated scattered fluxes as justification, as was done previously [3], we assessed the relative contributions of the different collision classes by fitting the measured fluxes of the different scattered charge states by

weighted linear combinations of the five identified collision types, in a manner similar to that outlined in Refs. 3 and 4. The obtained fits are shown as the solid lines in Figure 4. The scattered charge fractions resulting from the different contributing collision types could thus be deduced, as has already been discussed elsewhere [3]. The scattered charge fractions for the **SI** and **SII** collision type deduced in this manner are summarized in Table I, together with a comparison of the corresponding results for Ar^{9+} incident at 5 keV already presented in Ref. 4. A more complete tabulation that includes the other three collision types is deferred to a later publication.

When comparing the present measured and fitted charge fraction azimuth dependence for the 1+ scattered charge state with our previous results for 5 keV (see Ref. 4), it is noted that the sinusoidal modulation vs. azimuth seen at the lower energy is no longer evident. As discussed in greater detail in Ref. 4, this sinusoidal behavior implied a charge exchange process arising from a collective interaction with target rows along the [110] direction at distances that exceeded the MARLOWE collision criterion of 1.6 Å, and which therefore lay outside the scope of the MARLOWE simulation. Its absence at 20 keV supports the above-stated assumption that neutralization distances decrease with increasing energy, and provides some justification of decreasing the charge exchange critical distance below the MARLOW default value. An important conclusion from this discussion is that charge exchange (i.e. neutralization) critical distances in hard collisions must be determined independently of MARLOWE, and that the generally good agreement found at 5 keV, where the neutralization critical distance was in effect set equal to the MARLOWE b_{max}, may have been somewhat coincidental.

Simulation Sensitivity Studies

In this section we present some auxiliary simulation studies that explore the effects of changing the total scattering angle, details of the scattering potential, and type of surface reconstruction assumed. The first study was aimed at optimization of the scattering geometry specifically for a Au(110) surface. The second was carried out in part to assess the extent to which details of the azimuthal dependences were influenced by the scattered projectile charge states themselves. The third was undertaken to see what information about the surface topography itself the observed azimuth dependences of the scattered projectiles provided.

Total scattering Angle

When looking along the [110] direction, the reconstructed Au(110) surface has a characteristic projected opening angle of about 109^0. Ions with 10^0 incidence angle undergoing 120^0 backscattering thus seem well suited for probing the effects of the local corrugation of the missing row surface structure on projectile. In an attempt to find support for this intuitive picture, backscattering simulations were made for normal incidence in which the constraint of scattering into a particular detector solid angle was lifted, and all valid quasi-binary backscattering events were instead recorded by exiting polar and azimuthal angle. The result of this simulation, carried out at for 20 keV Ar projectiles, is shown in the top of Figure 7, where the number of events into a given direction is indicated by the greyscale to the right of the figure. The lower part of the figure shows three cuts of this data for three different total scattering angles, including the 120^0 at which the measurements were carried out. Interestingly enough, at the larger scattering angle of 140^0 the azimuthal variation of the total scattered flux has largely disappeared, while at the smaller scattering angle of 100^0 the azimuthal dependence shows much more complex oscillatory behavior with multiple periodicities. Both types of dependences would make

application of the fit procedure outlined above more problematic that was the case for 120^0. Since the 120^0 scattering angle in the present set-up was fixed in the design stage and is not easily changeable, Au(110) was, in hindsight, an excellent choice of target to investigate by this means.

Scattering Potential

The simulations used in our work to date used the ZBL [13] screened Coulomb potential appropriate for collisions between Au and Ar (i.e. Z_{Target} and $Z_{Projectile}$ equal to 79 and 18, respectively). In view of the progressively higher non-neutral scattered charge fractions observed as the projectile charge and/or energy are increased, we investigated possible effects on the simulated azimuth dependences of deviations from a pure screened Coulomb scattering potential. To this end we explored two changes in the scattering potential: simulating the effect of a surviving inner shell vacancy by increasing $Z_{projectile}$ to 19, and in a separate run adding to the ZBL potential a pure 1/R term (without screening), as a rather more extreme modification. The effects of both of these changes on the simulated azimuthal dependence of the scattered projectile flux is summarized in Figure 8. As can be seen, while the different scattering potentials result in some minor changes to the over-all azimuthal dependence of the scattered flux, no significant modifications result, when compared with the experimentally determined total flux distribution which has an estimated uncertainty of $\pm$ 15%, and considering the statistical uncertainty of the simulations, which comprised abut 200 events in the peak of the distribution. It is not clear whether the minor effect seen with the addition of the 1/R term is due to a true insensitivity of the overall scattering to this term, or to a limitation of MARLOWE, which treats the ion surface interaction as a series of binary collisions connected by straight line segments. It is noted that any periodicity that seems to be apparent in the simulation results is

artifically imposed, since the results were in fact only calculated between 0 and 90 deg, and then unfolded by assuming symmetry about the [110] and [100] directions.

Surface Reconstruction

An additional aspect we explored is the extent to which the (2x1) surface resonctruction of Au(110) manifested itself in the experimental and simulation results. To this end, we compared the simulated azimuthal dependences of scattered Ar projectiles incident normally at 5 keV on both reconstructed (i.e. having "missing rows") and unreconstructed (no "missing rows") Au(110) surfaces. As can be seen from Figure 9, there is a significant enhancement of quasi-binary scattering along the [100] direction, i.e. across the missing rows, which corresponds quantiatively with the doubling of the number of scattering lattice sites in the top layer when the missing rows are filled in. The excellent agreement of the reconstructed surface simulation results with our experimental data, carried out at samples temperatures in the range 300 – 450 K, confirms the expected (2x1) reconstruction of Au(110) at temperatures below the 650K phase transition [16].

Acknowledgements

This research was sponsored in part by the Office of Fusion Energy Sciences, and by the Office of Basic Energy Sciences of the U. S. Department of Energy under contract No. DE-AC05-00OR22725 with UT-Batelle, LLC. VAM was appointed through the ORNL Postdoctoral Research Associates Program administered jointly by Oak Ridge Associated Universities and ORNL.

TABLE I

Scattered charge fractions and the mean charge for **SI** and **SII** collisions from 20 keV Ar^{9+} incident projectiles normally incident on Au(110), compared to earlier results at 5 keV. Note that the 20 keV values were obtained from the modified fits, in which the maximum impact parameter for a charge exchange collision was reduced from the MARLOWE default value of 1.6 Å to 1.22Å.

	20 keV Ar^{9+}		*5 keV Ar^{9+}*	
Outgoing Charge State	***SI***	***SII***	***SI***	***SII***
0	0.24	0.80	0.37	1.00
+1	0.55	0.15	0.58	0.00
+2	0.17	0.04	0.042	0.00
+3	0.04	0.005	0.006	0.00
Mean charge	1.01	0.245	0.68	0.0

References

[1] W. Huang, H. Lebius, R. Schuch, M. Grether, and N. Stolterfoht, Phys. Rev. **A56**, 3777 (1997).

[2] W. Huang, H. Lebius, R. Schuch, M. Grether, and N. Stolterfoht, Phys. Rev. **A58**, 2962 (1998).

[3] V.A. Morozov and F.W. Meyer, Phys. Rev. Lett. **86**, 736 (2001).

[4] V.A. Morozov and F.W. Meyer, to be published in Phys. Scripta (HCI 2000 Conference proceedings).

[5] F.W. Meyer, V. A. Morozov, S. Datz, and R. Vane, to be published in Phys. Scripta (HCI 2000 Conference proceedings); F.W. Meyer, J. Mrogenda, V. A. Morozov, R. Vane, and S. Datz, this issue.

[6] Q. Yan, S. Schippers, D. M. Zehner, and F. W. Meyer, Phys. Rev. **A54**, 641 (1996); F.W. meyer, Q. Yan, P. Zeijlmans van Emmichoven, I. G. Hughes, and G. Spierings, Nucl. Instr. Methods Phys. Res. **B125,** 138 (1997).

[7] M.T. Robinson, Radiat. Eff. Defect. Solid. **130**, 3 (1994); Phys. Rev. **B40**, 10717 (1989).

[8] A. Arnau et al., Surf. Sci. Rep. **27**, 113 (1997), and references cited therein; HP. Winter and F. Aumayr, J. Phys. **B32**, R39 (1999), and references cited therein.

[9] F.W. Meyer and V.A. Morozov, Nucl. Inst. Methods Phys. Res. **B157**, 297 (1999).

[10] V. A. Morozov and F. W. Meyer, Rev. Sci. Inst. **70**, 4515 (1999).

[11] F.W. Meyer and V.A. Morozov, Phys. Scripta **T80**, 226 (1999).

[12] E .Taglauer, W. Englert, and W. Heiland, Phys. Rev. Lett. **45**, 740 (1980); T. M. Buck, G. H. Wheatley and L. K. Verheij, Surf. Sci. **90**, 635 (1970).

[13] J. F. Ziegler, J. P. Biersack and U. Littmark, The Stopping and Range of Ions in Solids. Vol.1, (Pergamon Press, New York, 1985), p.48.

[14] W. Moritz and D. Wolf, Surf. Sci. **88**, L29 (1979)

[15] R. Koch et al., Appl. Phys. **A55**, 417 (1992).

[16] J. C. Campuzano, M. S. Foster, G. Jennings, R. F. Willis, and W. Unertl, Phys. Rev. Lett. **54**, 2684 (1985).

FIGURE CAPTIONS

Figure 1. Experimental time-of-flight spectrum for Ar^{9+} normally incident on Au(110) at 20 keV, showing the scattered charge dispersion obtained by biasing the flight tube at –4.0 kV (thick lines), and the difference spectrum obtained by subtracting the corresponding grounded flight tube spectrum, used to eliminate much of the neutral multiple collision background, and to determine the detection efficiency of the MCP, as described in Ref. [10]. The curves shown are the results of non-linear multiple-Gaussian fits obtained using ORIGIN Pro 6.1, and illustrate the method of obtaining the peak areas for the various scattered charge states.

Figure 2. Simulation results of the energy distribution of scattered Ar projectiles incident on Au(110) normally at 5 keV in the [100] direction, i.e. across the missing rows. Note the quasi-binary double collision component at virtually the same energy as the binary collision peak at this azimuth. This is to be distriguished from the true double collision peak evident at higher scattered energies, discussed by, e.g. Ref. 1.

Figure 3. Simulation results of the azimuth dependence of each of the quasi-binary collision types, shown at the top of the figure, occuring in the first three target layers, for 5 keV Ar projectiles incident on Au(110) at 10^0.

Figure 4. Measured target azimuth dependence of scattered projectile charge fractions for 20 keV Ar^{9+} ions normally incident on Ar(110). The solid lines are fits to the different scattered charge states using MARLOWE simulation results as outlined in text.

Figure 5 Simulation results of the azimuth dependence of the different collision types indicated in the legends, occuring in the top three target layers (first three panels) for 20 keV Ar projectiles normally incident on Au(110) and using the MARLOWE default b_{max} collision

criterion for the neutralization critical distance. The fourth panel shows total simulated flux and comparison with experiment.

Figure 6. Same as Fig. 5, but using a neutralization critical distance of 1.22 Å.

Figure 7. (top) - Contour plot of the simulated scattered flux distribution over polar and azimuthal exit angles for 20 keV Ar projectiles normally incident on Au(110); (bottom) – cuts of the total flux azimuth distribution shown in the top plot at three different polar exit angles.

Figure 8. Simulated azimuth dependences of the total scattered projectile flux for 20 keV Ar projectiles using three different scattering potentials (see text).

Figure 9. Simulated azimuth dependences of the total scattered projectile flux for 5 keV Ar projectiles normally incident on a reconstructed (i.e. having "missing rows") and non-reconstructed (i.e. no "missing rows") Au(110) surface.

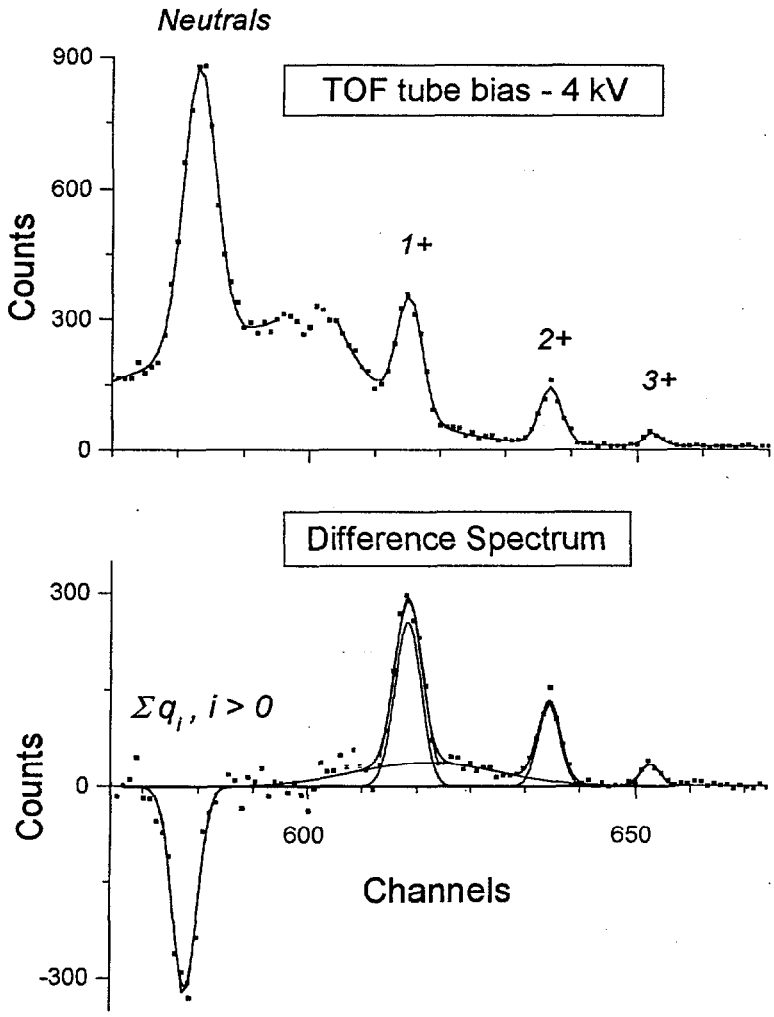
Neutrals
900
600
300
0
Counts
TOF tube bias - 4 kV
1+
2+
3+
Difference Spectrum
300
0
-300
Counts
Σq_i, $i > 0$
600
650
Channels

Figure 1

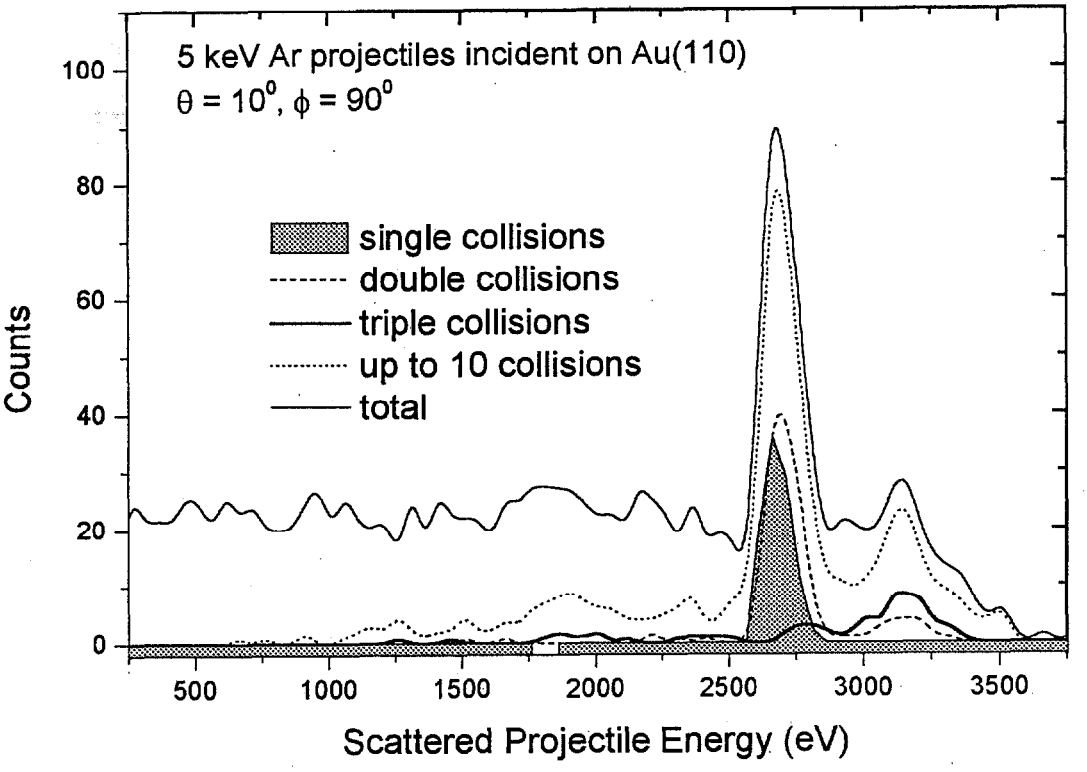
5 keV Ar projectiles incident on Au(110)
θ = 10°, ϕ = 90°
single collisions
double collisions
triple collisions
up to 10 collisions
total
Counts
Scattered Projectile Energy (eV)
0
20
40
60
80
100
500
1000
1500
2000
2500
3000
3500

Figure 2

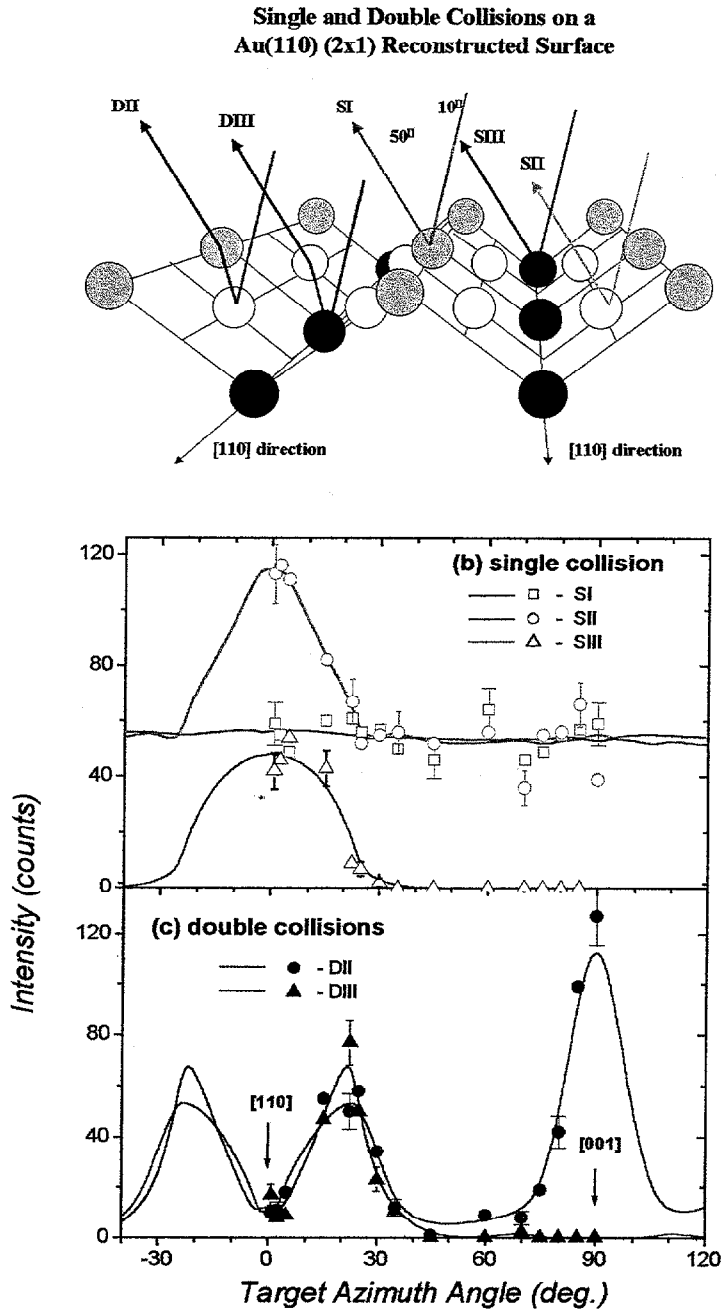
Single and Double Collisions on a
Au(110) (2x1) Reconstructed Surface
DII
DIII
SI
10°
50°
SIII
SII
[110] direction
[110] direction
(b) single collision
- SI
- SII
- SIII
(c) double collisions
- DII
- DIII
[110]
[001]
Intensity (counts)
Target Azimuth Angle (deg.)
120
80
40
0
-30
0
30
60
90
120

Figure 3

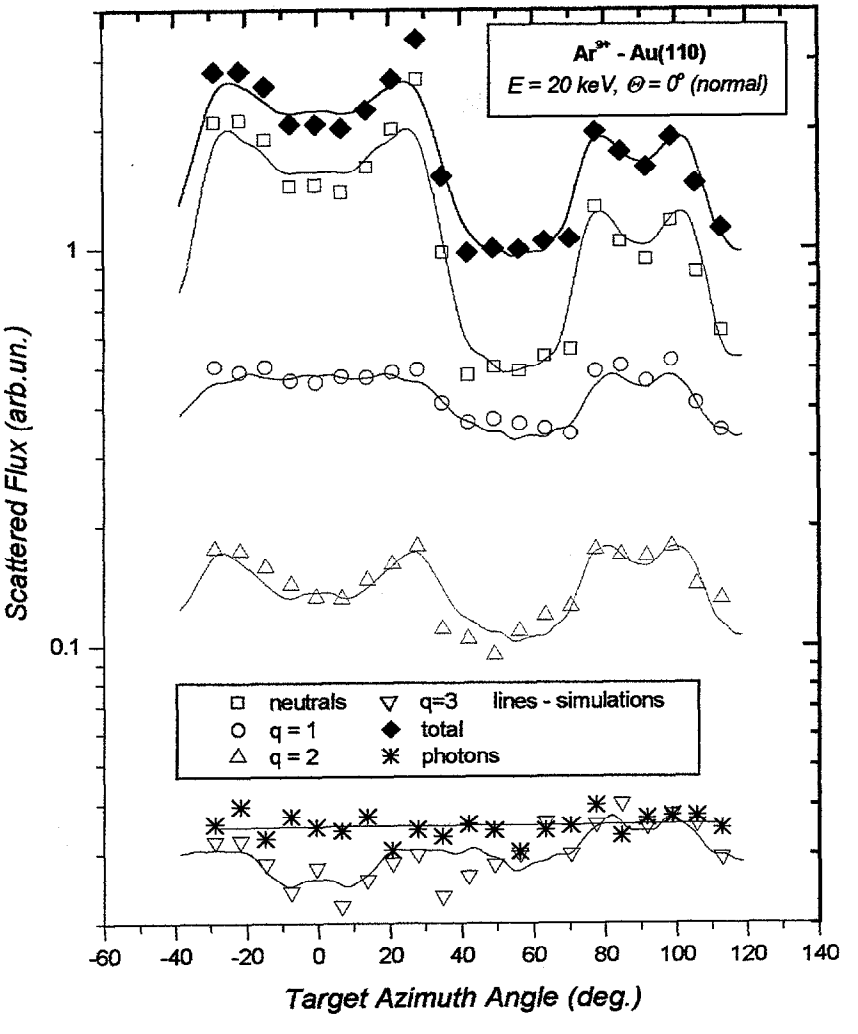
Ar9+ - Au(110)
E = 20 keV, Θ = 0° (normal)
1
0.1
Scattered Flux (arb.un.)
neutrals
q = 1
q = 2
q=3
total
photons
lines - simulations
-60
-40
-20
0
20
40
60
80
100
120
140
Target Azimuth Angle (deg.)

Figure 4

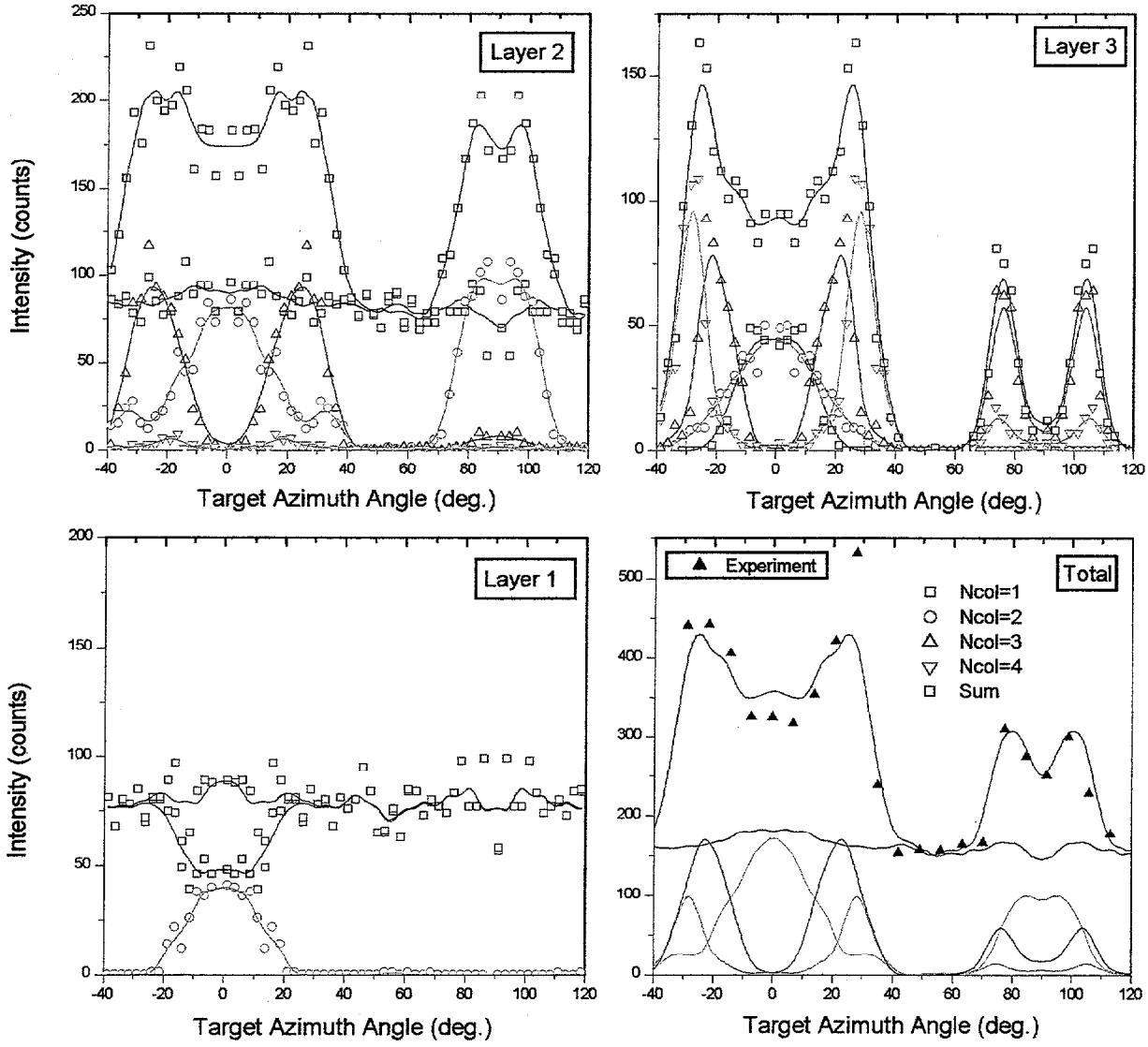
Layer 2
Layer 3
Layer 1
Experiment
Total
Ncol=1
Ncol=2
Ncol=3
Ncol=4
Sum
Intensity (counts)
Target Azimuth Angle (deg.)

Figure 5

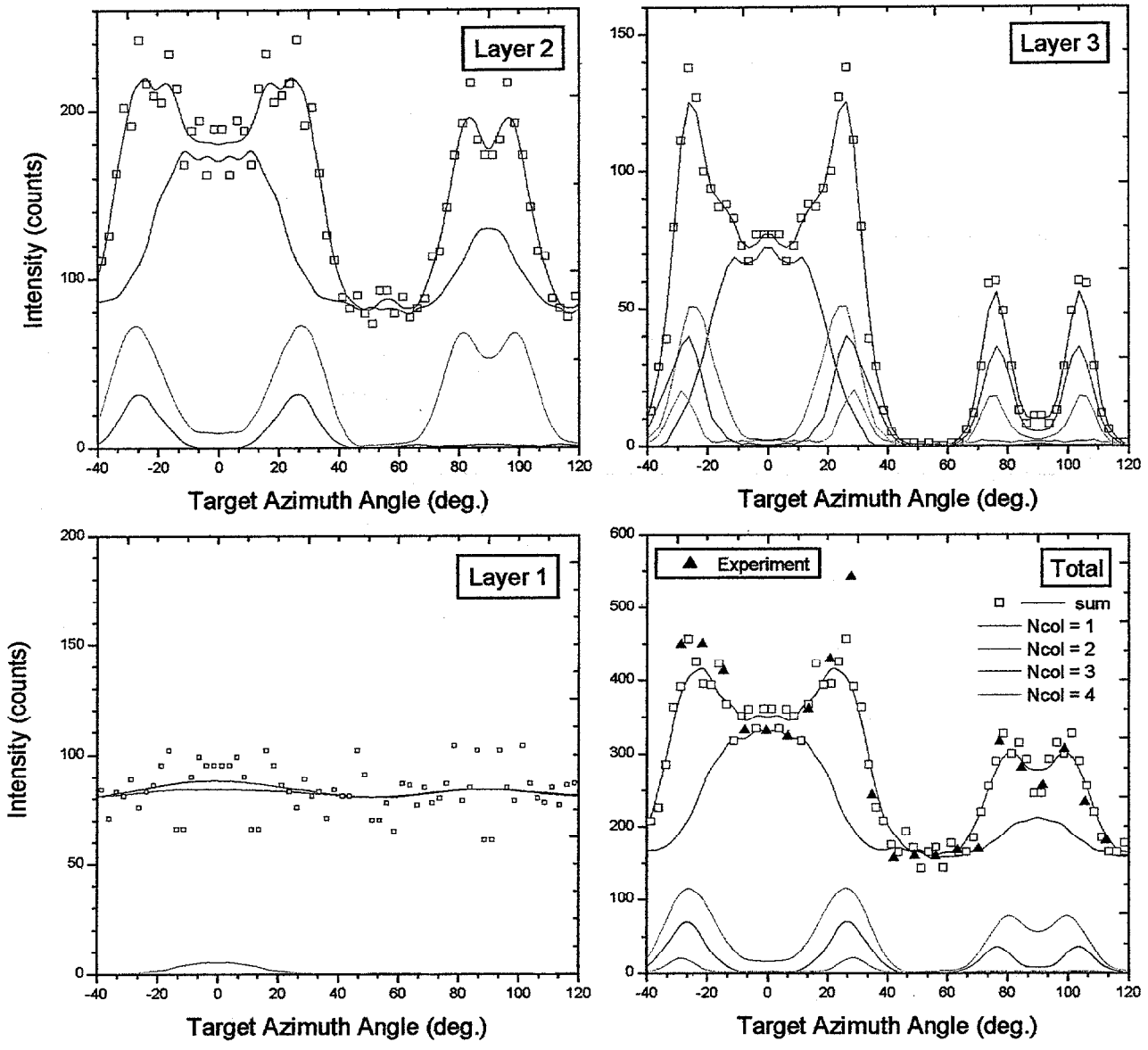
Layer 2
Layer 3
Layer 1
Total
Experiment
sum
Ncol = 1
Ncol = 2
Ncol = 3
Ncol = 4
Intensity (counts)
Target Azimuth Angle (deg.)

Figure 6

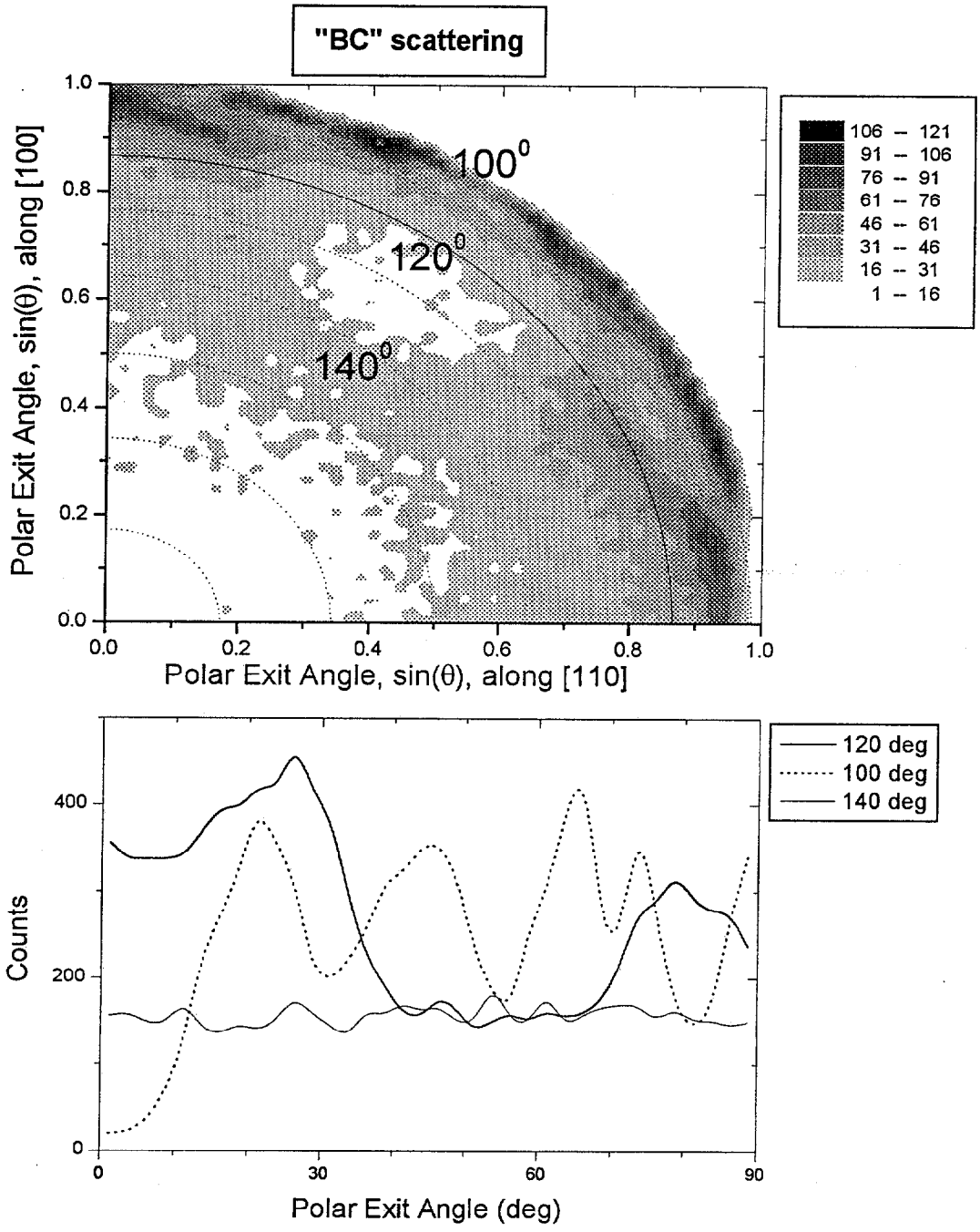
"BC" scattering
100⁰
120⁰
140⁰
106 – 121
91 – 106
76 – 91
61 – 76
46 – 61
31 – 46
16 – 31
1 – 16
Polar Exit Angle, sin(θ), along [100]
Polar Exit Angle, sin(θ), along [110]
0.0
0.2
0.4
0.6
0.8
1.0
120 deg
100 deg
140 deg
Counts
0
200
400
0
30
60
90
Polar Exit Angle (deg)

Figure 7

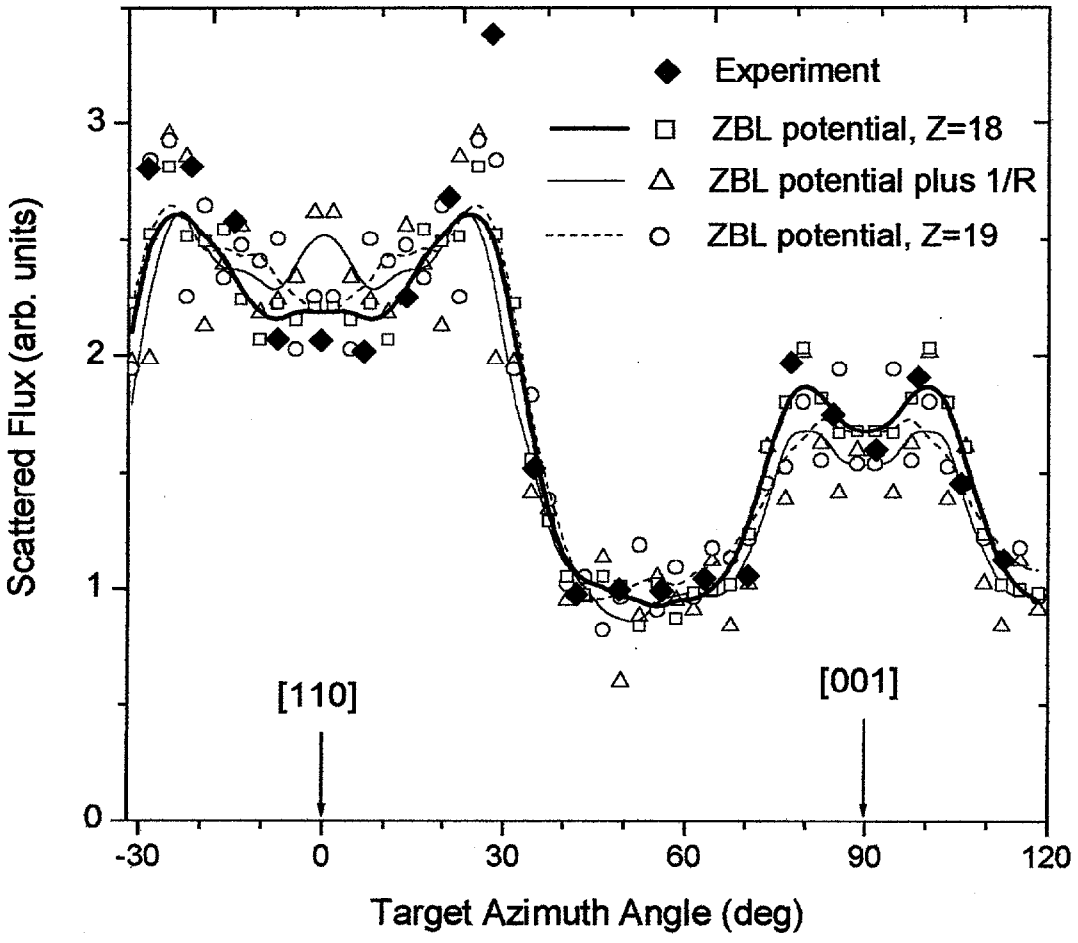
Experiment
ZBL potential, Z=18
ZBL potential plus 1/R
ZBL potential, Z=19
Scattered Flux (arb. units)
Target Azimuth Angle (deg)
[110]
[001]
0
1
2
3
-30
0
30
60
90
120

Figure 8

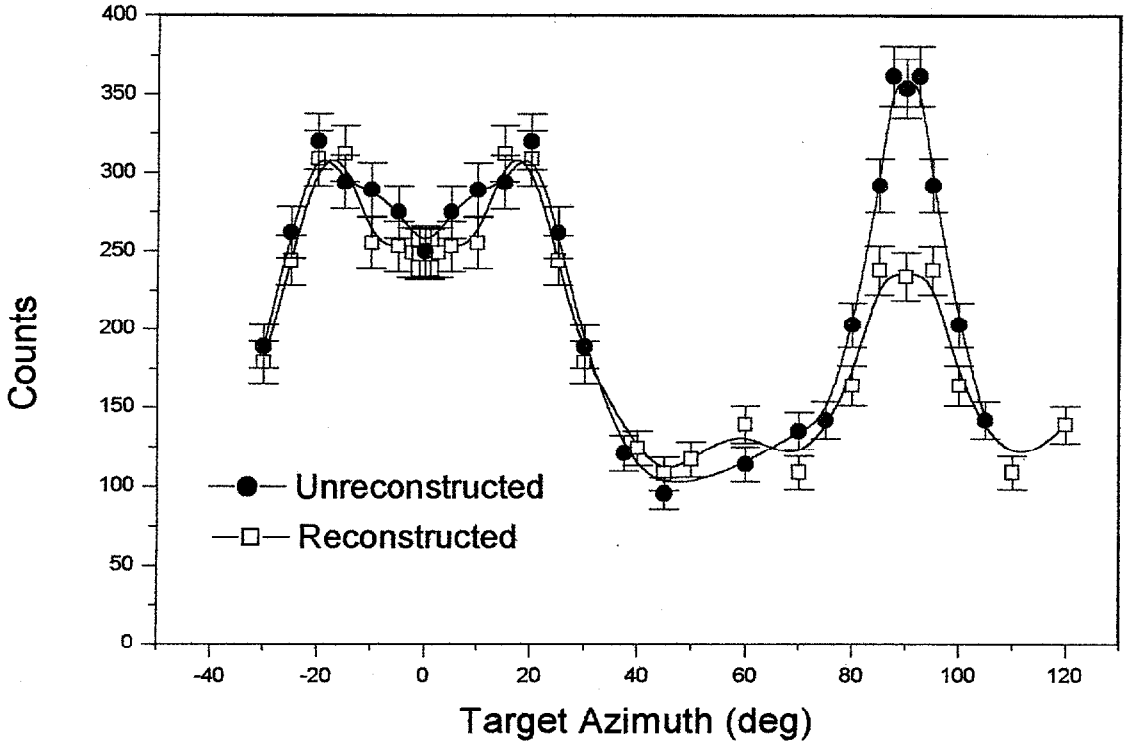
Counts
400
350
300
250
200
150
100
50
0
-40
-20
0
20
40
60
80
100
120
Target Azimuth (deg)
Unreconstructed
Reconstructed

Figure 9